

Holography at the ATA

G. R. Harp and R. F. Ackermann

3/21/4

Abstract

Beam patterns acquired from the offset Gregorian ATA dishes using prototype ATA feeds (electrically equivalent to final design apart from system temperature) are used to characterize the primary beam and can be used for holographic analysis of the dish surface. Because of the relatively low frequencies (1.5 – 2.3 GHz) used, very large areas of the sky must be sampled and a nontrivial mapping takes the data from (az, el) coordinates to coordinates appropriate for holographic inversion. The ATA dish has an ellipsoidal primary beam with low sidelobes. The sidelobes are especially low at large angles from the look direction, and highlight the effectiveness of the shroud surrounding the feed. Holographic inversion of the dish surface is tested using large fiducial letters that spell “ATA.” Holographic images clearly show the dish outline and uniform phase across the dish surface.

Introduction

It is desirable for the collecting surfaces of a radio telescope array to have shapes that produce a smooth primary beam with sidelobes that are low in amplitude, especially at large angles. This feature reduces the level of radio frequency interference that enters the receiver, and is very desirable for SETI searches where RFI can confound the measurement. Likewise, RFI and radiation from natural radio sources such as supernova remnants can degrade image fidelity in radio astronomy applications, and a beam pattern with low sidelobes simplifies data analysis.

The ATA offset Gregorian design was chosen partly because of its clear aperture, which leads to lower sidelobes than an obstructed aperture, as in a prime focus design. Additionally a metallic shroud around the ATA feed blocks the direct line of sight between the feed and the ground. In this memo we discuss initial beam pattern measurements with the ATA antennas. In these measurements, a prototype ATA feed (equivalent to the actual ATA feed but with higher system temperature) is the receiver for the experiment.

Experiment

We measured the beam pattern of ATA Antenna number 1 (A1) by cross correlating the signal received in that antenna with that from another antenna (A3). The signal source was a geostationary radio satellite (DARS XM-1) broadcasting at 2.3335 GHz (see Fig. 1).

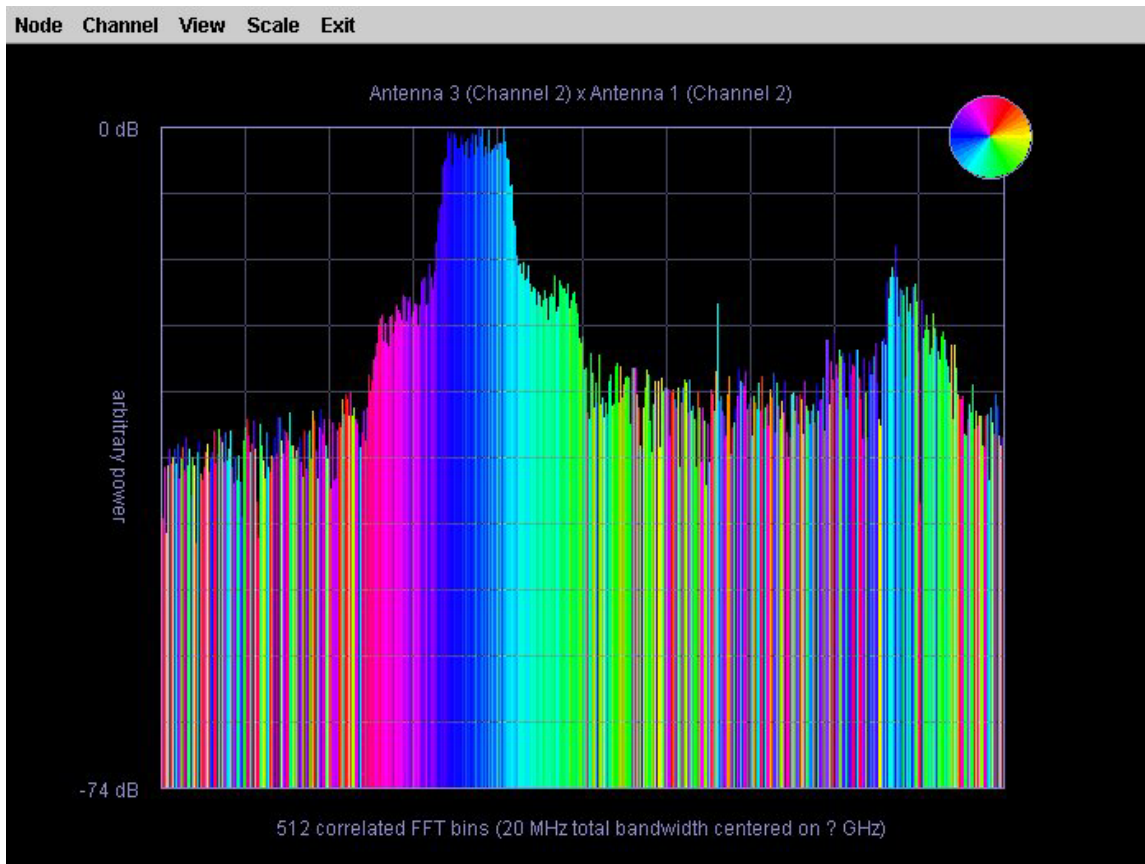


Figure 1: Integrated complex cross correlation of a single polarization of A1 and A3 while both were pointed at the satellite source. The horizontal frequency scale is centered at 2.336 GHz and is 20 MHz wide; the vertical scale is logarithmic (0 to -74 dB). The color scale represents the phase of the correlation as indicated by the color wheel at upper right. The main, flat-topped peak was isolated for beam pattern measurements.

Figure 1 shows a screen shot of the software correlator GUI, and displays the cross correlation of one (linear) polarization on A1 with one polarization of A3. Because the satellite broadcasts RHCP, both linear feed polarizations are sensitive to it. The vertical scale is logarithmic, and the main peak is centered at 2.3335 GHz and is about 20 dB higher than the first plateau around it. A companion peak at 2.346 GHz is attenuated by the band pass filter. The color scale represents the phase of the cross correlation. Because the signals are not in delay alignment, there is a monotonic phase gradient through the satellite peak of about 0.5 radians / MHz (path length difference ~ 24 m). In the measurements described here, this cross correlation was masked such that only a 2 MHz band centered on the main peak was accumulated.

The signals were converted to baseband with the RPA downconverter (bandwidth 20 MHz) and reduced with the ATA software correlator which has a throughput of about 1% of the 20 MHz band. At this frequency the ATA primary beam FWHM is about 1.5° . The reference antenna (A3 employing an RPA feed) was pointed directly at the satellite

throughout the measurement. A1 was swept over a dense grid pattern centered on the satellite position (azimuth 131.5° , elevation 30.0°).

The correlator dump rate was set to 1 Hz. The cross correlation (e.g. (A1 vertical polarization) \otimes (A3 vertical polarization) $\equiv V_{1v,3v}$) was normalized to the autocorrelation of the signal on A3 ($V_{3v,3v}$) to compensate for variations in the satellite output power. At regular intervals, A1 returned to point directly at the satellite where a calibration datum ($C_{1v,3v}$) was acquired. Subsequent measurements were normalized to this calibration until the next calibration point was acquired. To summarize, the complex beam amplitude $B_{1v,3v}$ was calculated as

$$B_{1v,3v} = \frac{V_{1v,3v}}{V_{3v,3v} C_{1v,3v}}. \quad [1]$$

We experimented with two methods for data acquisition. Initially the antenna was sent to points on a uniform grid in azimuth and elevation and data was collected only after the antenna had settled into position. This method was used for the data with the letters. Later the acquisition program was revised to acquire data “on the fly” as the antenna scanned at a uniform rate of 0.5° per second. Starting at the azimuth of the satellite (131.5°), an elevation is chosen and azimuth is scanned in a loop as in Fig. 2. Just before each loop, A1 returned to the satellite direction to acquire a calibration point. Loops were acquired with elevation spacing of 1° (two scan lines per degree) until a map of the entire sky was accumulated (about 1.5 days).

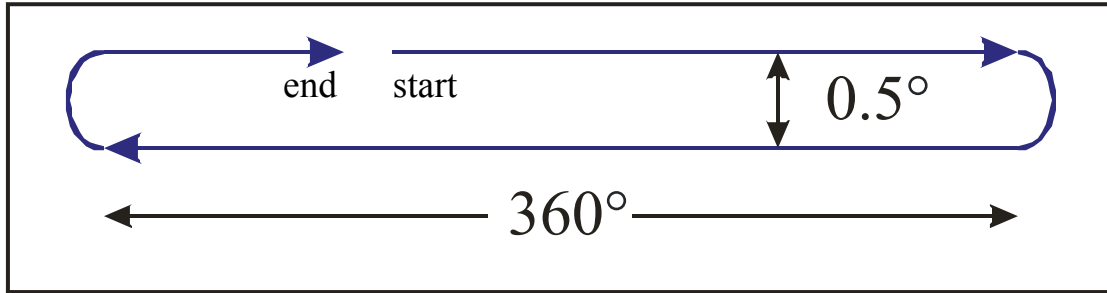


Figure 2: The blue curve indicates how the antenna is scanned in azimuth (horizontal) in a loop starting at the satellite azimuth. The elevation of the top and bottom of the scan is fixed and separated by 0.5° .

Figure 3 displays two all-sky power patterns taken with the “on the fly” method about 1 week apart. Notice that the color scale in this image spans a 60 dB range of power (30 dB in voltage). These images were generated from the raw measurements of Eq. [1] by convolving each datum with a Gaussian with $\text{FWHM} = 0.5^\circ$, and summing the results on a grid. While this sum is accumulating, a second grid is accumulated where each datum is replaced by unity. The latter grid provides a weighting factor. Finally, the data grid is divided by the weighting grid at all grid points within a radius of one primary beam HWHM of any actual data point. Grid points far from any actual data (i.e. low elevations)

are assigned a value of -60 dB (black). These images display some interesting structures which we shall return to below, but for now we observe that the data reproduce well.

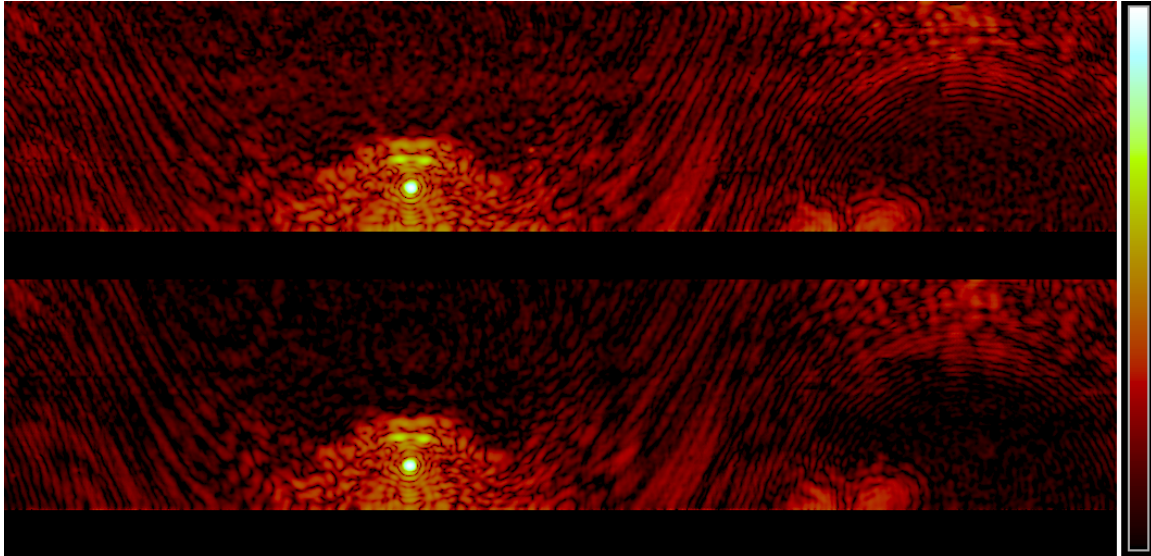


Figure 3: Two all-sky power patterns of the A1 vertical polarization taken on different days. The color scale varies over 60 dB in power units. In the upper image, $(az, el) = (0^\circ, 90^\circ)$ is at upper left and $(360^\circ, 0^\circ)$ is on the right hand side just where the lower image begins. The antenna cannot point below 17° elevation resulting in the black stripe at the bottom. Much of the detailed fine structure, 40 dB below the main peak, is reproduced in measurements separated by a week.

To move from the (az, el) grid in Fig. 3 to a holographic image of the dish is not trivial. For holography we wish to present the data on a hemisphere where the satellite position is at the center. One can think of holding the antenna fixed at zenith while the satellite is moved over all points in the sky. The mapping from Fig. 3 to holographic coordinates is neither unique (some points are represented twice) nor complete (some points are not represented at all). For a satellite at $(az, el) = (130^\circ, 30^\circ)$ (the approximate position of XM-1) the accessible range of holographic data is presented in Figure 4.

In this image, the red dot at the center represents a circle in the (az, el) grid. The large white circle is the “zenith circle,” where the elevation is 90° and the azimuth varies around the circle. The vertical yellow stripes are lines of constant azimuth, and the curved yellow stripes are lines of constant elevation. The pattern’s forward hemisphere inscribes the blue box.

Points below the red dot correspond to positions where the antenna points below the satellite (i.e. receiver “looks” above the pointing position). The curved band near the bottom corresponds to points near *zenith*, where the antenna is pointing 180° away from the satellite.

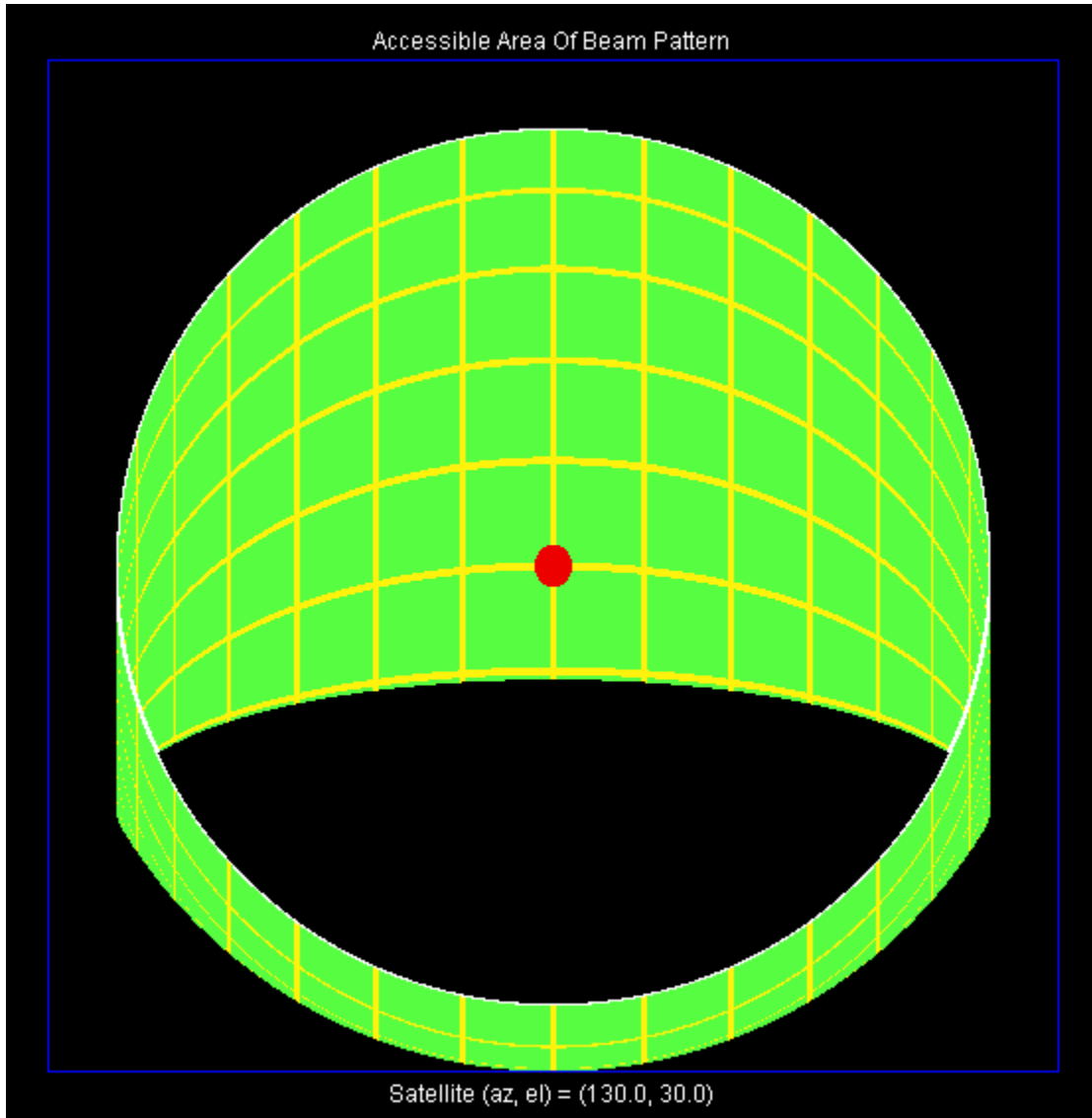


Figure 4: Visual representation of the angular distribution of holographic data that is available to an (az, el) antenna for a satellite positioned at 30° elevation. This figure also assumes a lower elevation limit of 17° as with ATA antenna 1. The yellow stripes represent lines of constant elevation (vertical) or constant azimuth (curved). Angles 90° from image center fall on a circle inscribing the blue box. Antenna zenith is represented in white.

In the next section, we apply this transformation to the data in Fig. 3 (bottom) to obtain beam patterns suitable for holographic transformation.

Results

Figures 5 and 6 show the beam patterns on the vertical and horizontal polarizations, respectively of A1 using the prototype ATA feed. In both figures, one discerns the trapezoidal opening in the metallic shroud as a region of elevated intensity. The wider opening above the feed appears at angles below the beam maximum. The shroud was

developed to shield the feed from ground radiation and scattering from adjacent antennas. We observe that it is also an effective barrier to line of sight radiation entering the feed directly from the satellite.

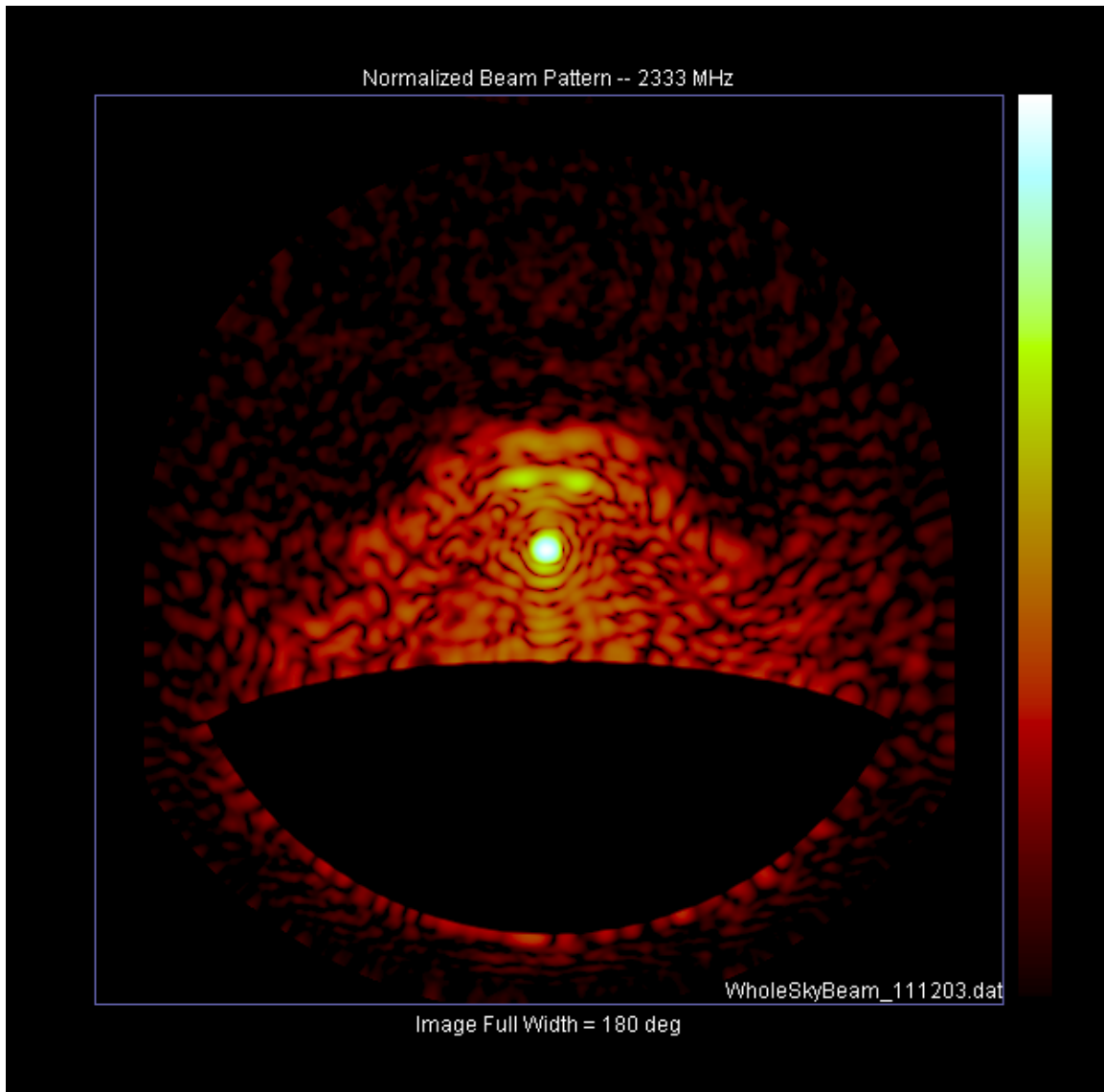


Figure 5: Power pattern of the vertical polarization on A1. Color scale spans 60 dB.

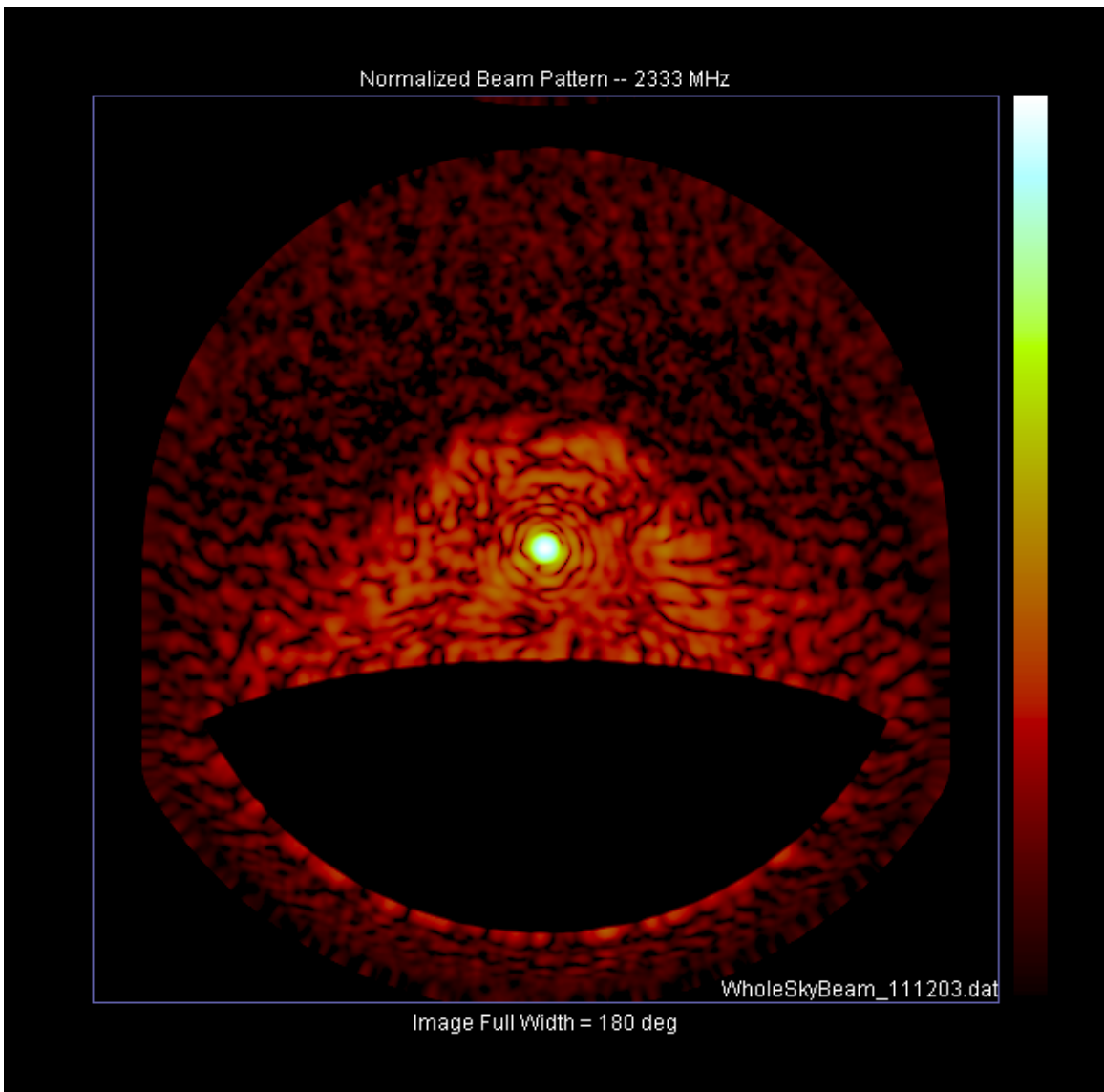


Figure 6: Power pattern of the horizontal polarization on A1. Color scale spans 60 dB.

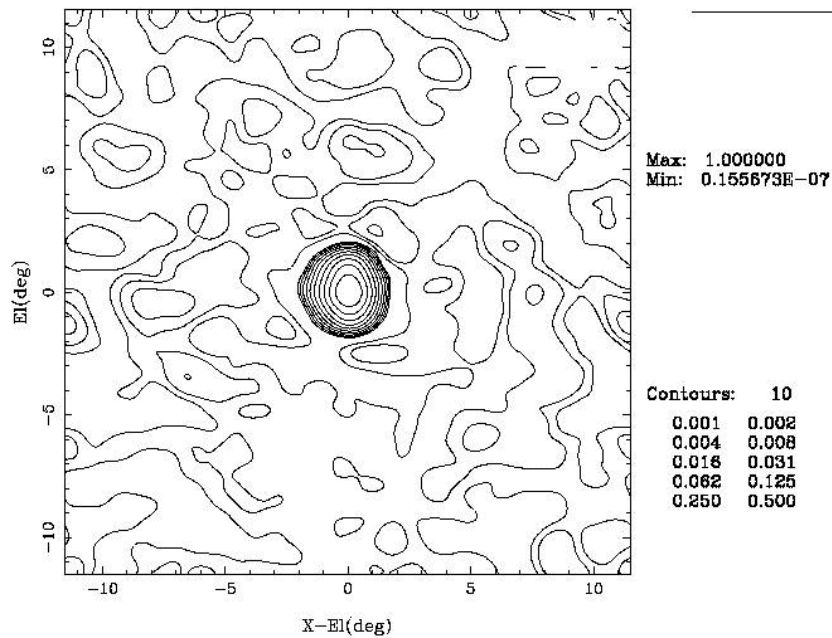
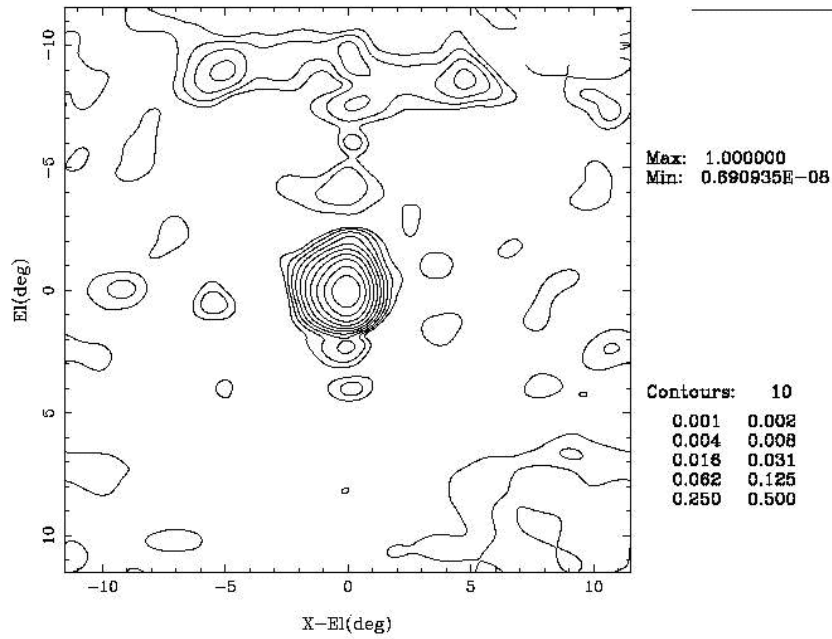


Figure 7: Contour plots of the central region of the beam pattern for the vertical polarization (top) and horizontal polarization (bottom).

In Fig. 7 we take a closer look at the central portion of each beam pattern. These contour plots show that the sidelobe power is below 1% everywhere away from the primary beam. Two strong coma features (the dog's sunglasses in Fig. 5) are visible in the vertical polarization 9° above the primary beam. Although these features are reproducible (see Fig. 3), they are not present in the horizontal polarization. Because they occur in the region of the shroud opening, they might be related to constructive interference of signals arriving on multiple paths.

While features like the shroud are most easily viewed in the mapping of Figs. 5 and 6, some are more apparent in the (az, el) mapping of Fig. 3. Returning to that figure, we point out two blobs at low elevation near $az = 270^\circ$. This is the direction where A1 is looking directly at A2, and might be related to scattering from that antenna. During the measurements, A2 was also pointed at the satellite so A2's focused satellite signal may be scattering off of some structure near its feed. This is a configuration where we have observed enhanced inter-antenna scattering in the past.¹

Backlobe Pattern

We notice in Fig. 3 a set of concentric circles appear centered at positive elevation but 180° away from the satellite position. While we anticipated some backlobe features, we initially expected them to be centered at negative elevation. However our intuition is guided by the properties of a symmetric telescope design. A symmetric primary surface presents a circular silhouette when it points directly away from the source ($el = -30^\circ$ here). Waves diffracting around the edge of such a dish will interfere constructively at all points on the dish axis.

But the ATA primary is an asymmetric ellipse cut from a much larger symmetric dish. Fig. 8 diagrams the situation in the spherical dish case. The circular asymmetric dish (blue) is cut from the symmetric dish (black) with center "c" and focus "f" as indicated. If we suppose the satellite is on the horizontal axis to the right of the figure, then the Airy diffraction axis of the black dish is horizontal. Constructive interference for the blue dish will occur along the red arrow, so we must tip it up by an angle θ to bring the arrow horizontal. Besides this effect, notice that the red arrow still does not intersect the receiver, effectively at "f". To bring the blue arrow horizontal we must tip the dish (about) twice as far, but this defeats the Airy diffraction condition. This intuitive analysis also neglects the shroud, which presents another diffracting edge of comparable importance. Thus it is difficult to predict the exact elevation angle about which the backlobe rings will be symmetric.

¹ Here we refer to an internally-published study of the shroud on A2. Experiments were performed with and without the shroud, measuring the signal on A2 while A1 was moved. Of all azimuthal directions, we saw the greatest scattering of a satellite signal from A1 when A1 was pointed directly at the satellite.

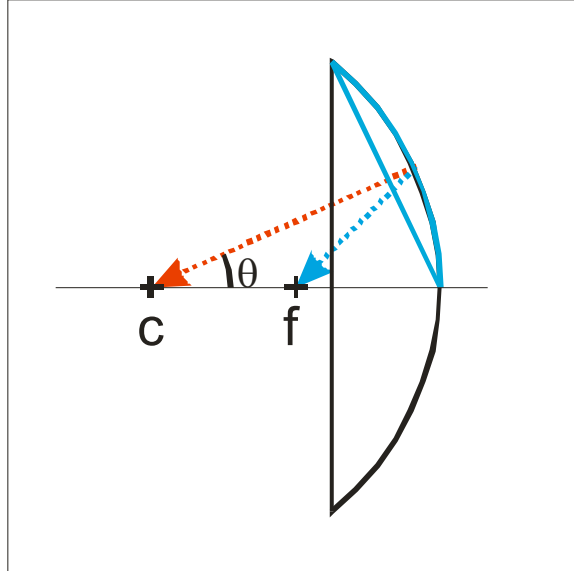


Figure 8: Diagram indicating the geometry for Airy diffraction for a spherical primary dish surface.

At the ATA, the plane of the primary circumference is tilted 29.4° to that of the fictitious symmetric primary dish.² We estimate that the backlobe center is shifted by approximately twice this angle, to $+28.8^\circ$ elevation. To test the validity of this analysis, Fig. 9 shows a mapping of the Fig. 3 data centered at $(az, el) = (311.5, 28.8)$. The blue cross indicates pattern center. Although the ring pattern is not circular, our simple analysis makes a reasonable estimate of the center of the backlobe pattern.

² The coordinates of the dish top and bottom in the coordinate system of the symmetric dish are $(5.78533, 0.0, -0.99911)$ and $(-0.304491, 0.0, 2.426415)$, respectively.

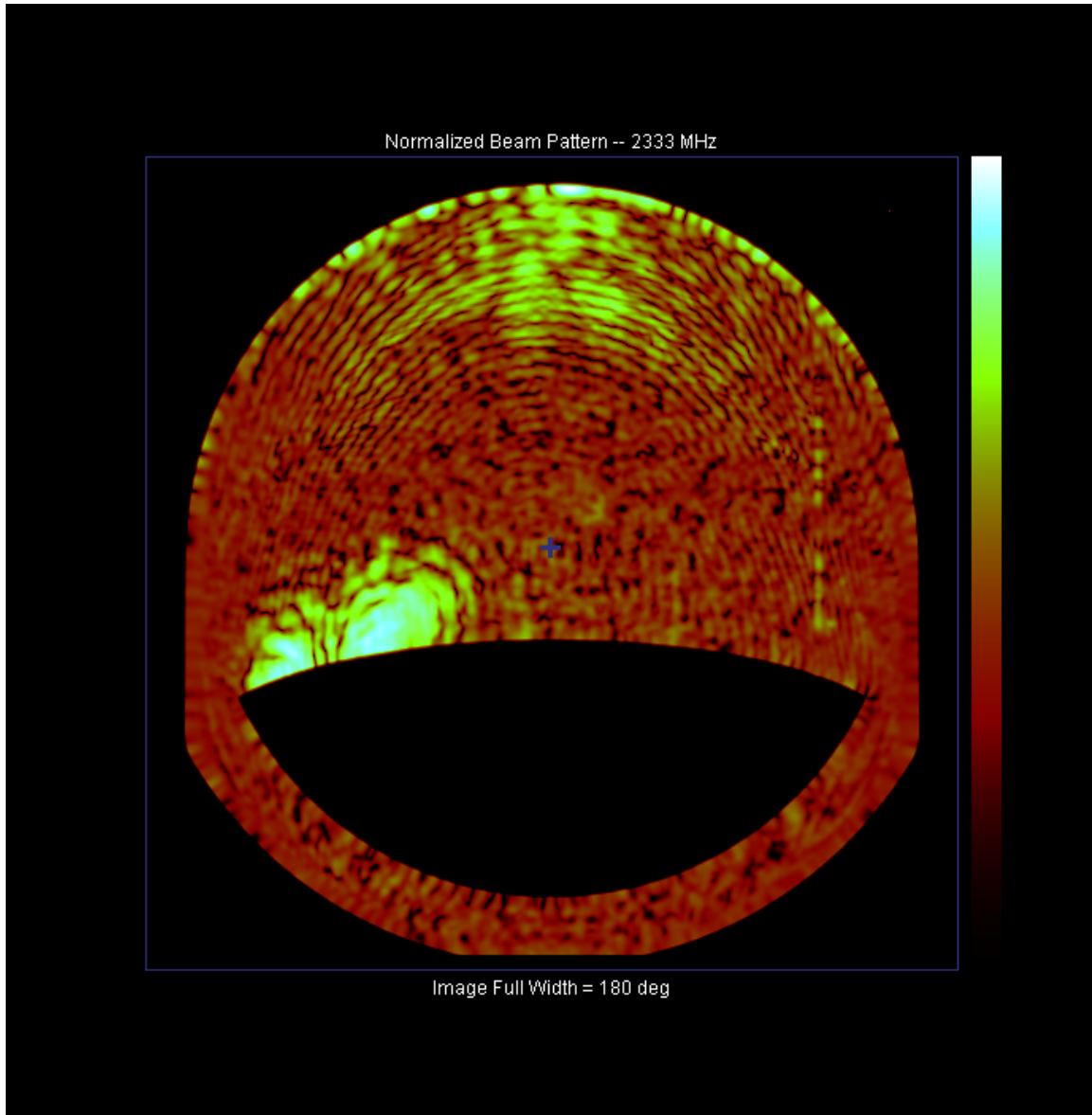


Figure 9: The data of Fig. 3 are remapped to be centered on the position (311.5, 28.8). Here a different color scale is chosen where the difference between maximum and minimum values spans 40 dB in power.

Holographic Analysis

The complex data from which Figs. 5 and 6 are derived can be Fourier transformed to reveal the primary dish illumination pattern. Because our measurement wavelength to dish diameter ratio (λ/D) is small by comparison to most radio telescopes, it is important to re-examine the theoretical basis for this kind of holography to be sure that no implicit assumptions are violated.

With large λ/D one need measure the beam pattern over only a small part of the sky that is well approximated by a plane. At the ATA the sidelobes (a.k.a. fringes) have a large

angular spacing so we must collect data over large solid angles. To obtain enough data to reasonably reconstruct the dish we must exceed the limits of the flat sky approximation.

At the other extreme, we have experimentally acquired data over most of the sky. One wonders how the information contained in the backlobe pattern should contribute to the analysis. Holographic analysis is based on a model of the telescope as a hole cut in a grounded conducting plane. In the time-reversed sense, electromagnetic waves emanate forward of this hole but from no where else on the plane. In this model, the beam pattern vanishes at 90° emission angle, and it has no meaning behind the plane. We conclude that without a more accurate model of the telescope geometry³ we cannot retain backlobe information in the holographic analysis.

Referring back to Fig. 8, we observe another complication. The optical axis of the ATA primary is angled 29.4° to its face. Holography gives the illumination pattern in the plane of the fictitious symmetric dish (black vertical line in figure) and not the plane of the ATA dish. Fortunately this is just what you want. When in focus there is a large vertical phase gradient across the face of the ATA dish, but one is really concerned with deviations from this gradient and not the gradient itself. By imaging in the plane of the fictitious symmetric dish we isolate the phase deviations of interest.

To review the holographic analysis, we imagine the telescope pointed along the z -axis and radiating while the beam pattern $B(\vec{k})$ is measured in the far field. At any point in the pattern, we define the wave vector $\vec{k} \equiv \frac{2\pi}{\lambda} \hat{k}$, where \hat{k} is a unit vector pointing from the dish to the measurement device. We can reconstruct the field amplitude $A(\vec{r})$ in the plane of emission using the Helmholtz-Kirchoff formula:

$$A(\vec{r}) = \int_{2\pi} B(\vec{k}) e^{-i\vec{k}\cdot\vec{r}} d\Omega. \quad (1)$$

For telescopes with large λ/D , the integral can be simplified by neglecting variation of the z -component of \vec{k} , but we don't do that here.

We analyze our discretely sampled data as follows. The position of each point is transformed into the holographic coordinate system (fig. 4). If the point is in front of the dish plane, it participates in a discrete Fourier transform according to equation (1) to give the raw dish image. At the same time, a second image of the ‘‘dish weight’’ is accumulated where $B(\vec{k})$ is replaced with unity. After all points have been considered, both images are multiplied by a Gaussian function with FWHM = 6 m (corresponding to a convolution of the beam pattern). Both images are fast Fourier transformed (FFT'ed) to

³The planar model is chosen to simplify the Greens function for the emitted wave, which gives rise to the $e^{-i\vec{k}\cdot\vec{r}}$ factor in Equation 1. To more accurately model the telescope, one must choose a different Greens function that contains information about the true shape of the dish. If you do this, however, Equation 1 will no longer be a simple Fourier transform.

the beam pattern plane, where the raw beam pattern is ratioed to the beam pattern weight⁴. This step gives uniform weight to each pattern point. The squared magnitude of this “Normalized Beam Pattern” is what we have plotted in Figs. 5 and 6. Finally the beam pattern is FFT’ed once again to give the normalized dish image.

ATA Letters

During the initial stages of analysis, it is convenient to place fiducials on the dish to verify the analysis programs. For fiducials, we used large aluminum letters spelling out “ATA” (Fig. 10). Although the letters appear large, typical features on the letters are only 3 wavelengths across, hence are barely resolved in the measurement. Each letter was backed by several pieces of 1” foam introducing a phase shift of nearly half a wavelength for waves scattering from the letters as compared with those from this dish. This maximizes the impact of the letters, especially in the phase image.



Figure 10: The human scale of the letters is shown, as well as their scale relative to the ATA primary dish.

Fig. 11 displays the reconstructed dish image with the letters in place. These images show the electric field intensity (left) and phase (right) in the plane of the fictitious symmetric dish (black section in fig. 8). The letters are easily seen. In the intensity image only the letter edge is apparent since this is where destructive interference takes place. The letter bodies are reflective and thus appear bright. In the phase image, the letters show striking contrast compared to their background. Because the letters are constructed of rather flimsy aluminum sheet, their distance from the dish surface undulates slightly between attachment points (barely visible in Fig. 10). The effects of this undulation are observed as color undulations in the phase image of Fig. 11.

The high fidelity of the letters reproduced in these images is a validation of our holographic analysis. For example, if we had not accounted for “curved sky” effects, the sharp edges of the letters in the phase image would not be resolved.

The square blemish on the lower right hand side of the dish is a calibration antenna that happened to be in place at the time. Its presence was fortuitous, since it allows us to

⁴ Points farther than one primary beam HWHM from any actual measured point are set to zero.

distinguish right from left (the letters are almost symmetrical). The data for these images were acquired on nearly rectangular grids which give rise to false images above, below, left and right of the true image.

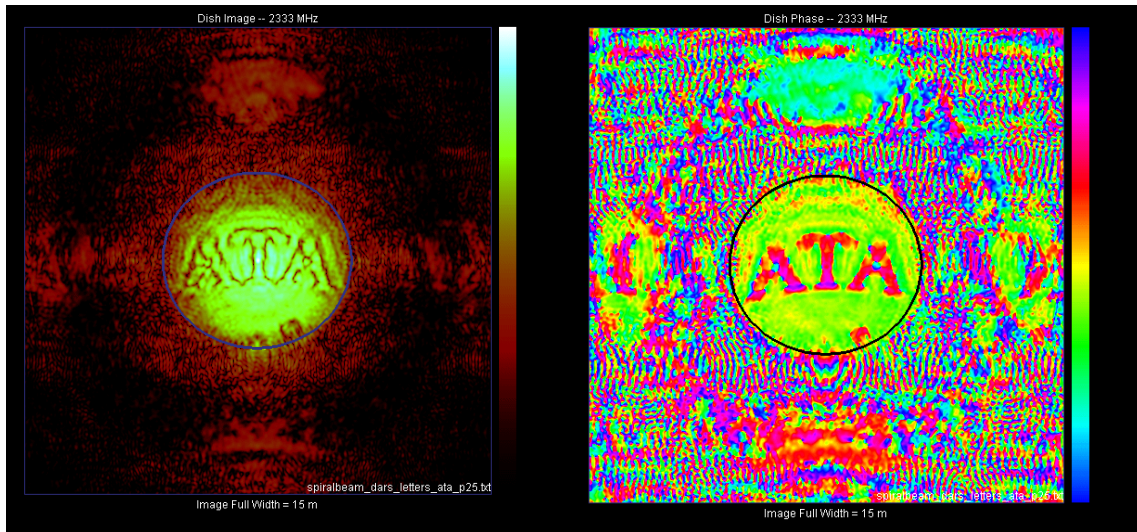


Figure 11: Dish intensity (left) and phase (right) obtained from beam patterns taken with the letters in place. On the left the color scale varies over 50 dB, while on the right it varies over 2π .

Holographic Analysis

The data of figs. 5 and 6 were Fourier transformed to give the electric field intensity (left) and phase (right) in figs. 12 and 13. The dark blue circle shows the outline of the ATA primary dish projected into this plane. The dish outline is clearly delineated in the measured image. Inside the dish aperture the electric field intensity is high enough to allow a good determination of the phase where its angular variation is less than π over the whole dish.

We pause to highlight the success implied by these images. The dish illumination pattern fills the primary dish. It tapers smoothly dropping to approximately 1% at the dish edge. This validates the feed illumination pattern and the optics of the secondary dish. Apart from some perturbations we discuss below, the phase is fairly uniform, which further validates the optics including primary surface.

Some ringing is apparent at the base of the dish in all images. In this area the waves are grazing the top of the secondary dish as they approach the primary. Additionally, the feed is attached to the primary surface in this area. Scattering of waves from either of these structures could account for this effect.

Horizontally aligned arcs spread vertically across the dish surface in Fig. 12. This is likely due to the coma features in Fig. 5. The two coma features are 9° from the primary maximum, corresponding to a spatial wavelength of 0.82 m. Thus we expect ~ 7 oscillations across the dish image in Fig. 12, just as we observe. The perturbations in Fig.

13 are weaker and less well organized, consistent with the fact that no strong secondary maxima appear in Fig. 6.

There is also a weak horizontal phase gradient of approximately 0.5 radians/meter in Fig. 12 that is not present in Fig. 13. This corresponds to a pointing squint of 0.6° between the two polarizations (about 40% of primary FWHM). This squint is evident in the raw beam pattern data as well, though it remains unexplained. It cannot be related to the coma features mentioned above since the horizontal spacing of these two features is too large to be consistent with this effect.

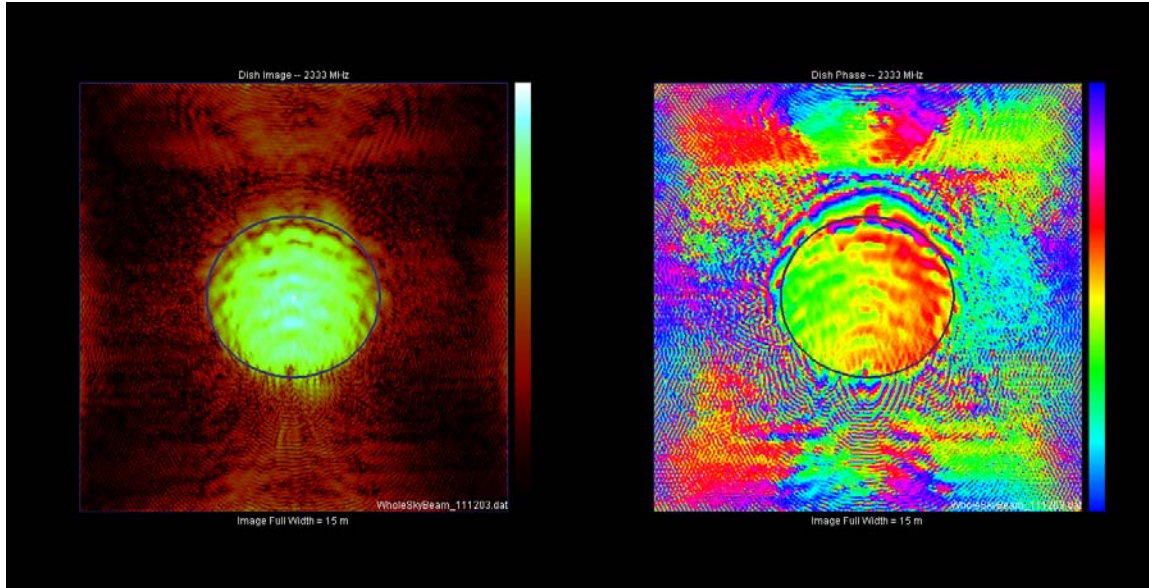


Figure 12: Dish power (left) and phase (right) for the vertical polarization. For power, the color scale is logarithmic spanning 60 dB; for phase the scale is linear and spans 2π .

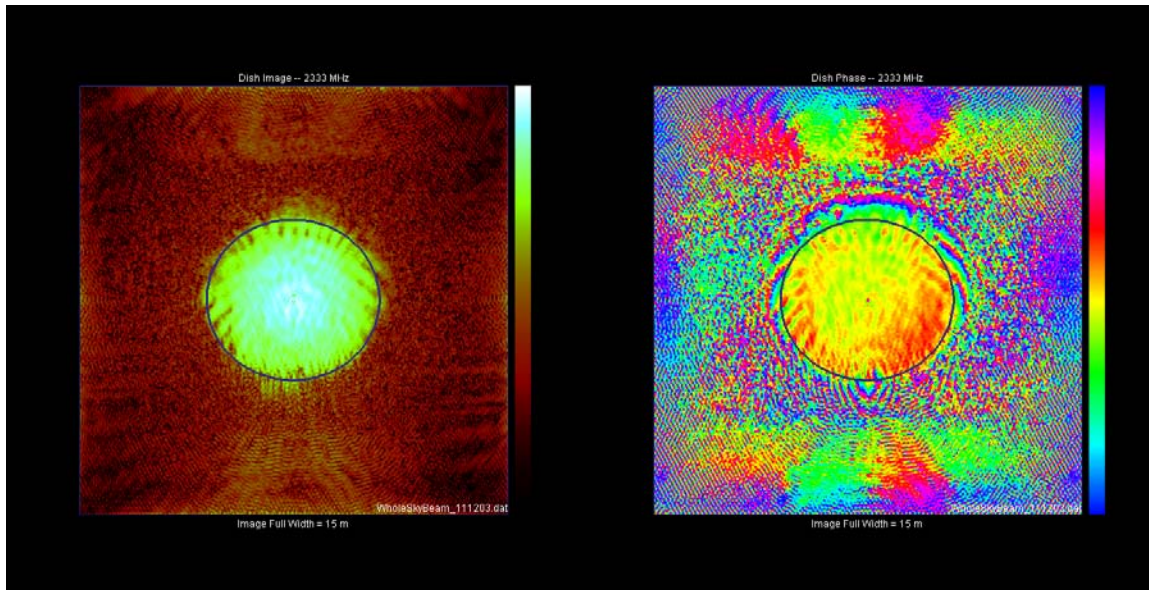


Figure 13: Same as fig. 12 but for horizontal polarization.

There is a weak radial phase gradient in Fig. 13 which is equivalent to a slight defocus of the feed. This defocusing might also be present in Fig. 12 but is obscured by the squint. Although the feed was placed at the nominal focus position for this measurement, small focus displacements are not surprising since we have no experience with this new design. Future measurements should systematically measure the focus as a function of frequency, which we hope will be transferable from one to all antennas, since they are nominally identical.

Using these dish illumination patterns above, we can characterize the primary dish illumination pattern, including contributions from the feed and secondary. First we fit the illumination power pattern for the vertical polarization with a 2-D Gaussian in Fig. 14. A similar fitting was performed on the horizontal polarization. The fitting parameters and semi-major and minor axis lengths of the projected dish are shown in Fig. 15. Along both axes, the Gaussian σ is about half the semi-major (minor) radius, consistent with design.

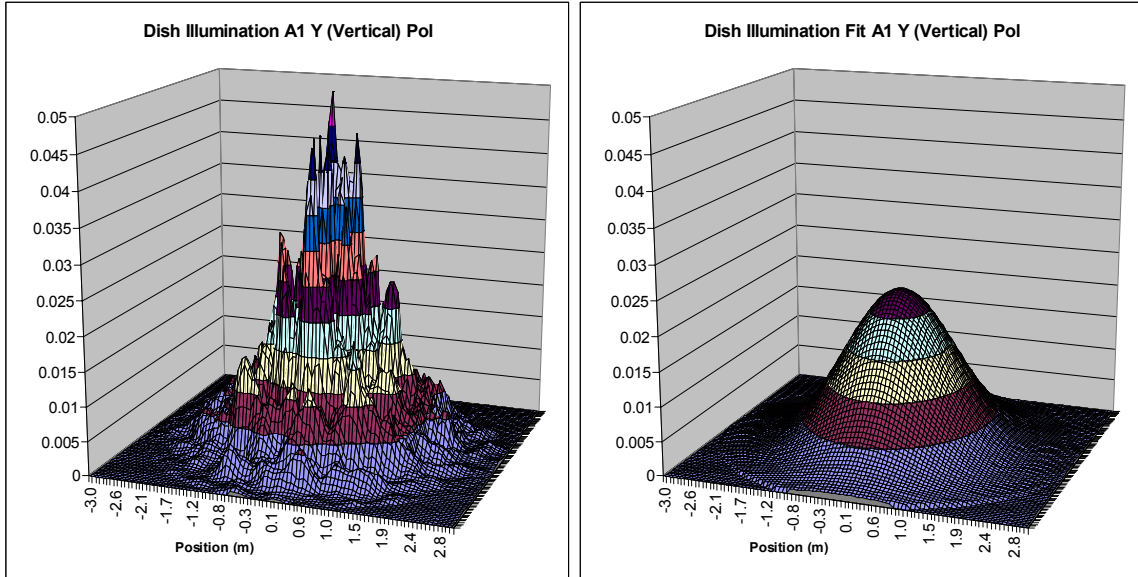


Figure 14: The dish illumination power pattern (left) is fit with a 2-D Gaussian profile (right). The vertical scale is linear, arbitrary units.

Gaussian Fit	σ_x	σ_y	Semi-major axis / 2	Semi-minor axis / 2
Vertical Pol	1.6 m	1.3 m	3.0 m	2.8 m
Horizontal Pol	1.4 m	1.4 m	3.0 m	2.8 m

Figure 15: Fitting parameters for Gaussian fits to power illumination patterns.

The dish illumination gives a direct measurement the effective area A_e (neglecting ohmic and matching losses), or the aperture efficiency, $\varepsilon = A_e / A$ where A is the dish area. A_e is calculated from

$$A_e = \frac{\left| \int A(x, y) dx dy \right|^2}{\int |A(x, y)|^2 dx dy}, \quad (2)$$

where $A(x, y)$ is the dish illumination pattern. Before applying Eq. 2, we must first correct for possible pointing offsets (e.g. the squint in the vertical polarization). We do this by multiplying $A(x, y)$ by a function $e^{i(k_x x + k_y y)}$ where k_x and k_y are chosen to maximize A_e . Actually, this correction is only a 1% effect, even for the vertical polarization. Pursuing Eq. 2, we find $\varepsilon_v = 55\%$ and $\varepsilon_h = 57\%$. This is very close to the expected value of 59% in the ATA design.

Conclusions

We conclude that the first ATA antenna is behaving quite well and in accordance with its design. Using a feed that is electrically identical to the final design (apart from system temperature), we have measured illumination patterns and aperture efficiencies (55%, 57% for vertical, horizontal, respectively) that are close to design values.

A few features remain unexplained, however. There is a noticeable pointing squint between the beam maxima for the two polarizations of about 0.6° . In the vertical polarization beam pattern only, there is a moderately strong coma feature which leads to phase and intensity modulations of the dish illumination pattern for that polarization. Future measurements will confirm and further characterize these features, but for now it is fair to say that the dish is operating well.

In a future paper, we intend to compare the present results to theoretically calculated results.

Acknowledgements

The authors gratefully acknowledge Lynn Baker, Mel Wright and David DeBoer for helpful discussions regarding the analysis and interpretation of these data.